Neurobiology of Disease

Toll/Interleukin-1 Receptor Domain-Containing Adapter Inducing Interferon-β Mediates Microglial Phagocytosis of Degenerating Axons

Suneil Hosmane,[1]* Million Adane Tegenge,[2]* Labchan Rajbhandari,[2] Prech Uapinyoying,[2] Nishant Ganesh Kumar,[1] Nitish Thakor,[1] and Arun Venkatesan[2]

Departments of [1]Biomedical Engineering and [2]Neurology, The Johns Hopkins University School of Medicine, Baltimore, Maryland 21287

Following CNS injury, microglial phagocytosis of damaged endogenous tissue is thought to play an important role in recovery and regeneration. Previous work has focused on delineating mechanisms of clearance of neurons and myelin. Little, however, is known of the mechanisms underlying phagocytosis of axon debris. We have developed a novel microfluidic platform that enables coculture of microglia with bundles of CNS axons to investigate mechanisms of microglial phagocytosis of axons. Using this platform, we find that axon degeneration results in the induction of type-1 interferon genes within microglia. Pharmacologic and genetic disruption of Toll/interleukin-1 receptor domain-containing adapter inducing interferon-β (TRIF), a Toll-like receptor adapter protein, blocks induction of the interferon response and inhibits microglial phagocytosis of axon debris *in vitro*. *In vivo*, microglial phagocytosis of axons following dorsal root axotomy is impaired in mice in which TRIF has been genetically deleted. Furthermore, we identify the p38 mitogen-activated protein kinase (MAPK) cascade as a signaling pathway downstream of TRIF following axon degeneration and find that inhibition of p38 MAPK by SB203580 (4-(4-fluorophenyl)-2-(4-methylsulfinylphenyl)-5-(4-pyridyl)-1H-imidazole) also blocked clearance of axon debris. Finally, we find that TRIF-dependent microglial clearance of unmyelinated axon debris facilitates axon outgrowth. Overall, we provide evidence that TRIF-mediated signaling plays an unexpected role in axonal debris clearance by microglia, thereby facilitating a more permissive environment for axonal outgrowth. Our study has significant implications for the development of novel regenerative and restorative strategies for the many traumatic, neuroinflammatory, and neurodegenerative conditions characterized by CNS axon degeneration.

Introduction

Microglia are the resident immune cells of the CNS and play a major role in pathogen defense, inflammatory responses, and phagocytosis (Napoli and Neumann, 2009; Ransohoff and Perry, 2009). Although microglial phagocytosis of pathogens is often coupled to elaboration of proinflammatory molecules with resulting neurotoxicity, phagocytosis of apoptotic cells usually proceeds without signs of inflammation or neurodegeneration and is essential for normal development, tissue homeostasis, and recovery from acute injury (Voll et al., 1997; Fadok et al., 1998). The phagocytic clearance of myelin debris by microglia is also important for CNS repair (Dubois-Dalcq et al., 2005; Franklin and Kotter, 2008). However, microglial phagocytosis of endogenous debris can be extremely inefficient in the mammalian CNS, and the resultant persistence of endogenous debris poses a substantial barrier to regeneration (Vallières et al., 2006; Neumann et al., 2009). Thus, it is critical to understand mechanisms by which microglia clear debris, to develop strategies to enhance repair.

Emerging evidence points to remarkable diversity in phagocytic mechanisms (Napoli and Neumann, 2009). The Toll-like receptors (TLRs), which signal through several Toll–interleukin-1 receptor (TIR) domain-containing adapter proteins including myeloid differentiation response protein-88 (MyD88) and TIR domain-containing adapter inducing interferon-β (TRIF) (O'Neill and Bowie, 2007), play an important role in phagocytosis of microbes. Microglial clearance of apoptotic neurons, however, involves TIM-4 (T-cell Ig mucin 4), a phosphatidyl serine receptor, as well as soluble bridging proteins such as milk fat globule-EGF-factor 8 and Gas6 that couple apoptotic cells to microglia (Miyanishi et al., 2007; Grommes et al., 2008). Another cell surface receptor, triggering receptor expressed on myeloid cells 2 (TREM2), has also been recently implicated in phagocytosis of apoptotic neurons and suppression of inflammation (Takahashi et al., 2005). In addition, distinct receptors and signaling pathways govern microglial removal of myelin debris (Rotshenker et al., 2008).

Little, however, is known about the molecular control of microglial phagocytosis of degenerating axons. CNS axonal degen-

Received Jan. 14, 2012; revised April 24, 2012; accepted April 25, 2012.

Author contributions: S.H., M.A.T., N.T., and A.V. designed research; S.H., M.A.T., L.R., P.U., and A.V. performed research; N.T. and A.V. contributed unpublished reagents/analytic tools; S.H., M.A.T., L.R., P.U., N.G.K., and A.V. analyzed data; S.H., M.A.T., and A.V. wrote the paper.

This work was supported by the Johns Hopkins Institute for Nanobiotechnology (N.T., A.V.), National Institutes of Health Grant 1F31NS066753-01 (S.H.), National Institute on Drug Abuse Grant K08DA22946 (A.V.), and Howard Hughes Medical Institute Early Career Physician–Scientist Award (A.V.). We thank April Ruffin for technical assistance and Daphne Hutton for her artistic help.

*S.H. and M.A.T. contributed equally to this work.

Correspondence should be addressed to Arun Venkatesan at the above address. E-mail: avenkat2@jhmi.edu.

DOI:10.1523/JNEUROSCI.0203-12.2012

 0270-6474/12/327745-13$15.00/0

eration is a common occurrence in many disorders including multiple sclerosis (MS), where early axonal injury can occur with relative sparing of distant neuronal cell bodies (Coleman, 2005; Pittock and Lucchinetti, 2007). Following acute injury, axonal debris persists for many months in the CNS (Bignami et al., 1981; George and Griffin, 1994). Moreover, axon debris is generated on an ongoing basis in chronic disorders such as MS, where degenerating axons have been found in both active and chronic lesions (Trapp et al., 1998). Studies of phagocytosis of axonal debris in *Drosophila* have demonstrated an essential role for the glial engulfment receptor Draper, and its intracellular signaling partner Shark, suggesting a role for the ITAM (immunoreceptor tyrosine-based activation motif)-domain-SFK (Src family kinase)-Syk signaling cascade in axonal phagocytosis (Ziegenfuss et al., 2008). In addition, activation of the p38 mitogen-activated protein kinase (MAPK) cascade has been recently implicated in clearance of axonal debris by microglia (Tanaka et al., 2009). Here, we develop a novel compartmentalized microfluidic coculture platform to study microglial–axon interactions, and uncover an unexpected role for TRIF in mediating microglial clearance of degenerating axons.

Materials and Methods

Microfluidic axon–microglia coculture platform. An extracellular matrix patterning device was used to create 25-μm-wide stripes of poly-D-lysine (PDL) separated by 25-μm-wide spaces to facilitate areas for axonal outgrowth and microglia attachment, respectively (see Fig. 1*Ai*). The PDMS [poly(dimethylsiloxane)]-based microfluidic device is composed of two [length (L), 8 mm; width (W), 1 mm] compartments separated by an array of 150 microchannels [W, 25 μm; L, 5 mm; height (H), 5 μm] and was fabricated as previously described (Taylor et al., 2005; Hosmane et al., 2010). The patterning device was attached to a cleaned glass-bottom Petri dish (Wilco Wells) and a 200 μg/ml solution of PDL (Sigma-Aldrich) diluted in molecular grade water (Mediatech) was introduced by way of access ports. The ensemble was then incubated overnight at 37°C in a humidified, 5% CO_2 incubator. The following day, the devices were slowly peeled from the glass substrate, and the dish was washed three times with double-dionized water to remove unbound PDL. After drying, a similar device with 120 miniaturized microchannels (W, 10 μm; L, 500 μm; H, 2.5 μm) was aligned and bonded to the PDL-patterned glass through the use of alignment keys (see Fig. 1*Aii*). As previously described for unpatterned substrates (Hosmane et al., 2010), neurons seeded within the cell body compartment extend axons, a subset of which are guided along the microchannel features and enter into the axon–glial coculture compartment. In our patterned platform, the axons remain spatially localized after emerging from the microchannels (see Fig. 1*Aiii*), thus allowing a clear demarcation between axon bundles and spaces for glial coculture (see Fig. 1*Aiv*). We took advantage of this property to develop a reproducible assay to quantitatively assess clearance of axonal material.

Cell isolation and culture. Primary hippocampal neurons were obtained from rat embryonic day 17 pups as previously described (Hosmane et al., 2010) and resuspended to a final density of 2.5×10^7 cells/ml, in Neurobasal/B27 media. For experiments in which cells were labeled with a fluorescent protein, dissociated neurons were nucleofected (Amaxa) with a plasmid encoding the tau-TdTomato gene as per the manufacturer's instructions. Efficiency of labeling was >50%. For primary microglia cultures, cortices from P3–P6 Sprague Dawley rats (Charles River Laboratories) or C57BL/6J mice (The Jackson Laboratory) were isolated and digested in 0.05% trypsin (Invitrogen) for 20 min at 37°C. Trypsinization was stopped by equal volume of DMEM/F12 media (DMEM/F12 from Mediatech; 1% penicillin–streptomycin from Invitrogen; and 10% FBS from Gemini Bio-Products). Next, the cell suspension was filtered through a 100 μm cell strainer and centrifuged. Finally, the cell pellet was resuspended in DMEM/F12 media and plated in poly-L-lysine-coated T-75 culture flasks, and medium was changed every 4 d. For our experiments, microglia were isolated on days 7 (rat) and 14 (mouse) by shaking flasks at 180 rpm at 37°C for 45 min and were enriched by plating on uncoated plastic/glass surfaces. Under these conditions, >95% of isolated cells stained for the microglia marker Iba1.

Mouse peritoneal macrophages were isolated from wild-type (wt) and TRIF knock-out (TRIF KO) mice, 4 d after intraperitoneal injection of 2 ml of sterile 3% (w/v) thioglycolate (Sigma-Aldrich; T9032) (Zhang et al., 2008). Macrophages were further purified by passing through a MACS cell separator column with CD11b beads (MACS; Miltenyi Biotec), following which flow cytometry demonstrated >95% CD11b-positive cells. Axon debris clearance experiments were performed as described for microglia.

Neuron–microglia coculture and axon degeneration. Devices were filled with prewarmed Neurobasal/B27 media for 15–30 min before cell seeding. Primary neurons were loaded into the cell body compartment of the device, and axons were observed entering the axon/coculture compartment after 3–4 d. After 7 d, 50,000 microglia were loaded into the coculture compartment in 1.5 μl of 2% serum-containing media (DMEM/F12, 2% FBS, 1% antibiotics). After 30 min, the coculture compartment was washed once and filled with DMEM/F12/2% FBS media. A fresh 1 M solution of diethylammonium (*Z*)-1-(*N*,*N*-diethylamino)diazen-1-ium-1,2-diolate (DEANONOate) (Cayman Chemical) was prepared by dissolving 50 μg of stock powder into 50 μl of ice-cold 0.01 M NaOH. To induce neuronal degeneration, 15 μl of 10 mM DEANONOate was immediately added to the cell body compartment such that the overall volume was at least seven times less than that of the coculture compartment. Under these conditions, no detectable diffusion of NO (Promega; Griess Assay) into the coculture compartment was observed.

Microarray. RNA was isolated from coculture compartments via the RNeasy Plus Mini Kit (QIAGEN), as per the manufacturer's directions. RNA was then labeled using the Whole Transcript Sense Target Labeling protocol described by Affymetrix with reagents from Ambion and Affymetrix. Briefly, 100 ng of total RNA was used to synthesize first-strand cDNA using random oligonucleotides with T7 promoter as primer and the SuperScript Choice System (Invitrogen). Following the double-stranded cDNA synthesis, the double-strand cDNA was purified using magnetic beads, and cRNA was generated through *in vitro* transcription. Ten micrograms of cRNA were then used to generate sense strand cDNA using random primer, dNTP-dUTP mix, and SuperScript II reverse transcriptase (Invitrogen). The resulting sense strand cDNA was then purified, fragmented using UDG (uracil DNA glycosylase) and APE (apurinic/apyrimidinic endonuclease) at 37°C for 60 min, and terminal labeled with biotinylated nucleotide and terminal DNA transferase at 37°C for 60 min. The labeled sense strand DNA was hybridized to the Affymetrix GeneChip rat exon 1.0 ST arrays for 17 h at 45°C with constant rotation (60 rpm). Affymetrix Fluidics Station 450 was used to wash and stain the chips, removing the nonhybridized target and incubating with a streptavidin–phycoerythrin conjugate to stain the biotinylated cDNA. The staining was further amplified using goat IgG as blocking reagent and biotinylated anti-streptavidin antibody (goat), followed by a second staining step with a streptavidin–phycoerythrin conjugate. Fluorescence was detected using the Affymetrix G3000 GeneArray Scanner and image analysis of each GeneChip was performed through the Affymetrix GeneChip Command Console, version 2.0 (AGCC, version 2.0), software from Affymetrix. Data analysis was performed using Partek Genomic Suite software. In short, the raw signal values are background corrected using RMA and quantile normalized. Differential gene expression was detected using ANOVA and visualization and further functional analysis was performed using Spotfire Functional Genomic DecisionSite.

Quantitative PCR. Fifty nanograms of each mRNA sample was converted to cDNA using the High-Capacity RNA-to-cDNA kit (Applied Biosystems). cDNA was subjected to TaqMan PCR using the gene expression master mix containing TaqMan primers (Applied Biosystems) to genes of interest and actin primer (Predeveloped TaqMan Assay Reagents). The reaction mix was run on an ABI Prism 7000 Sequence detection system and analyzed. In some experiments, microglia were cultured in a 48-well plate at 2×10^5 cells per well and treated with either TLR3 agonist (20 μg/ml polyinosinic/polycytidylic acid [poly(I:C)]; InvivoGen), TLR4 agonist (100 ng/ml lipopolysaccharide; Sigma-Aldrich),

or microbeads (FluoSpheres; Invitrogen; 2×10^6 per well) before collection of mRNA.

Immunocytochemistry. Cultures were washed with PBS and fixed for 20 min at room temperature with 4% paraformaldehyde (PFA). Cells were washed in PBS and incubated in blocking solution containing 0.25% Triton X-100 and 5% normal donkey serum for 1 h. Primary antibodies, which included rabbit IBA-1 (1:500; Wako Chemicals), rabbit IRF7 (1:250; Santa Cruz Biotechnology), mouse β-III-tubulin (1:1000; Source), and rabbit phospho-p38 MAPK (1:250; Cell Signaling), were diluted in blocking solution and applied overnight at 4°C. Cultures were washed three times in PBS and incubated with Alexa Fluor 488-conjugated donkey anti-rabbit (1:250; Invitrogen) and Alexa Fluor 594-conjugated donkey anti-rat (1:250; Invitrogen) for 2 h at room temperature. Finally, cells were incubated for 5 min with 1 μM 4′,6-diamidino-2′-phenylindoldihydrochloride (DAPI) (Invitrogen) as a nuclear counterstain.

Western blotting. Cultures were washed with 1× Dulbecco's PBS (DPBS) (Mediatech). DPBS was removed from the coculture compartment and replaced with RIPA lysis buffer. Lysates from the coculture compartments of several devices were pooled and stored on ice. The protein level of the lysate was determined by the BCA protein assay kit (Thermo Fisher Scientific). Twenty micrograms of protein per lane were separated by 10% SDS-PAGE and transferred onto a nitrocellulose membrane overnight. After blocking with 10% milk in PBS and Tween 20 for 30 min, membranes were incubated for 3 h at room temperature with primary rabbit antibody (1:1000 phospho-p38 MAPK; Cell Signaling). After washing, horseradish peroxidase-conjugated anti-rabbit (1:5000; GE Healthcare) antibody was applied for 45 min at room temperature. Antibody binding was detected using chemiluminescence HRP for 5 min and visualized by fluorography with film. The total level of p38 MAPK was detected from the same blot after stripping with 1× of Re-Blot Plus Strong Solution (Millipore) in distilled water for 15 min, followed by reprobing with p38 MAPK antibody (Cell Signaling).

Pharmacological blockers. The peptides Pepinh-MyD, Pepinh-TRIF, and Pepinh-Control (InvivoGen) were prepared as 1 mM stock solutions by dissolving peptides in endotoxin-free water and used at final concentrations of 10 and 20 μM. Microglia were preincubated for 6 h with the peptides before stimulation with exogenous ligands or degenerating axons. The p38 MAPK inhibitor (4-(4-fluorophenyl)-2-(4-methylsulfinylphenyl)-5-(4-pyridyl)-1H-imidazole) (SB203580); Sigma-Aldrich] was prepared as a 50 mM stock solution in DMSO (dimethylsulfoxide). Microglia were preincubated with SB203580 at final concentration of 50 μM for 1 h before experimentation.

Determination of intra-axonal ATP. Intra-axonal ATP was determined by using ViaLight Plus Kit (Lonza). Briefly, cultures were washed once with DPBS, and DPBS was added to fill the cell body compartment. Fifty microliters of cell lysis buffer were then added to the axonal compartment and incubated for 10 min at room temperature. The axonal lysates were collected, added to a white-walled luminometer plate (Lonza), and mixed with AMR PLUS (Lonza). Bioluminescence was measured within 5 min in a SpectraMax M5 plate reader (see Fig. 1*C*; Molecular Devices).

Time-lapse microscopy. Bright-field and phase-contrast video micrographs were captured at 40× magnification with a Zeiss live-cell inverted microscope (Axio Observer; Zeiss) using Zeiss AxioVision software. Images were acquired at fixed time increments (3 min) under constant exposure (<150 ms). Due to the fine temporal resolution of image capture, clear assessment of axonal health (continued growth vs degeneration) could be determined (see Fig. 1*B*). Time-lapse microscopy was used for >16 h after induction of axonal degeneration to observe the cellular response of microglia cocultured with axon bundles (see Fig. 1*D*).

Quantification of axon debris clearance. Axon bundles (W, >20 μm; L, >500 μm) surrounded by >10 microglia were selected for time-lapse microscopy and subsequent quantification. The surface area of the axon bundles were traced at the start of the experiment immediately after the addition of 10 mM NO donor to the neuronal cell bodies. At the end of the experiment (16–18 h later), axon bundles were traced again to quantify the extent of debris clearance by microglia. Surface area quantification was done manually in Zeiss AxioVision through the use of a multiline segment tracing tool. The difference in bundle surface area normalized to the area at the start of the experiment was quantified and then stated as the percentage of axon debris cleared (see Fig. 1*D*). For each experimental condition, a minimum of three bundles was quantified per device sector, and at least three sectors were analyzed per experiment. Each experiment was then performed in triplicate. Data were then analyzed by one-way Tukey's ANOVA in Prism (GraphPad) to determine statistical significance. Unless otherwise stated, all columns were compared against the positive control, which was microglia cocultured with degenerating axons ($^*p < 0.05$; $^{**}p < 0.01$; $^{***}p < 0.001$).

The percentage of microglia phagocytosing axon debris *in vitro* was quantified as follows. TdTomato-labeled axons were cocultured with wt or TRIF KO microglia. Neurons were subjected to NO-induced degeneration, and cultures were fixed and immunostained for Iba1 and counterstained with DAPI at 16 and 24 h after NO donor application. At least five random areas at 40× magnification were imaged per sector by confocal microscopy, at least four independent sectors were analyzed per experiment, and the percentage of Iba1$^+$ cells that colocalized with TdTomato was determined by orthogonal analysis as in Figure 1*E*. Overall, at least 500 Iba1$^+$ microglia were analyzed per condition, and the experiment was performed in duplicate.

Axon outgrowth through axonal debris. Microfluidic platforms were modified to allow unrestricted access to the axonal compartment, thereby allowing collection of axonal material. After 7 d in culture, axon bundles were subjected to axotomy by mechanical cutting. Axonal material was scraped and collected, and cellular membrane debris from human embryonic kidney (HEK) 293 cells was collected in a similar manner. Axonal and HEK cell material were subjected to three cycles of freezing at −20°C followed by thawing at 37°C to promote debris formation, which resulted in debris aggregates ranging from 1 to 10 μm in diameter. Debris were concentrated and applied at a final concentration of 2500 particles/μl to the axonal compartments of 3- to 4-d-old neuronal cultures in which axons had not yet extended into the axon compartment. Axonal outgrowth into the axonal compartment was followed by time-lapse microscopy. In some experiments, microglia (wild-type or TRIF knock-out at density of 2500 cells/μl) were cultured along with axonal debris in the axonal compartment of 3- to 4-d-old neuronal cultures. New axon bundles were allowed to grow into the axonal compartments for 3 d, followed by fixation and immunostaining for β-III-tubulin. The longest axon in each axon bundle was measured, and at least 100 bundles per condition were quantified in each experiment. Experiments were done in triplicate.

Dorsal root axotomy. Eight-week-old male TRIF KO mice or wt C57BL/6J controls (The Jackson Laboratory) were used in this study. Dorsal root axotomies were performed on mice deeply anesthetized with isoflurane. Hemilaminectomies were performed to expose the cauda equina, followed by cutting of the L2–L4 roots just proximal to the dorsal root ganglion. The wounds were closed with sutures, and the animals were allowed to recover. All experiments and procedures were approved by the Animal Research Committee of The Johns Hopkins University School of Medicine. Animals were transcardially perfused with cold PBS followed with 4% paraformaldehyde. After overnight postfixation, spinal cords were immersed in 30% sucrose and kept at 4°C for at least 24 h. The spinal cord was removed from the L2 region, using the sacrum and ribs as landmarks, and cut into 35 μm sections using a cryostat. Immunohistochemistry was performed as previously described (Lee et al., 2011). Sections of both genotypes were labeled at the same time using the same solutions, but in different wells so that sections could be identified following unblinding. Briefly, free-floating tissue sections were washed with PBS, and then preincubated in blocking solution (1× PBS with 5% donkey serum and 0.2% Triton X-100) for 1 h. Primary antibodies were diluted in blocking solution as follows: anti-IBA1 (1:500; rabbit; Wako), anti-Lamp1 (1:250; rat; Developmental Studies Hybridoma Bank), and anti SMI31/32 (1:2500; mouse; Abcam), and incubated overnight at 4°C. After washing with PBS, slices were incubated with the appropriate fluorescent-conjugated secondary antibody (1:250; Jackson ImmunoResearch Laboratories) and counterstained with DAPI. Slices were mounted, dried, and imaged using a Zeiss Meta 510 confocal microscope. *Z*-stacks (1 μm thick) were constructed for each image. In the dorsal

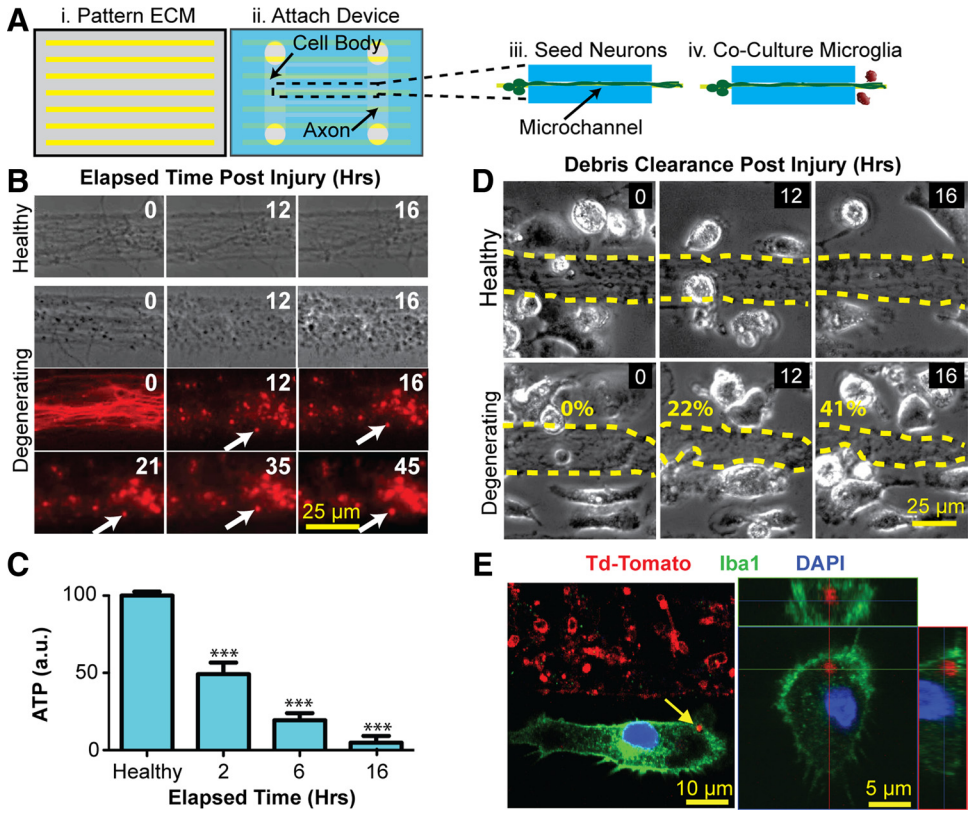

Figure 1. Novel microfluidic platform enables the study of microglial phagocytosis of axons. ***Ai***, A patterning process was used to create 25-μm-wide PDL stripes interspersed by 25 μm gaps. ***Aii***, The microfluidic coculture device was aligned and bonded. ***Aiii***, ***Aiv***, Neurons cultured within the cell body compartment extended axon bundles through the microchannels and into the axon/glial coculture compartment (***Aiii***) where microglia were later cocultured (***Aiv***). ***B***, Application of nitric oxide (NO) to the cell bodies led to morphologic changes consistent with axon degeneration and the formation of stable (>45 h) axon debris fragments (white arrows). ***C***, Intra-axonal ATP decreases in a time-dependent fashion following NO application. Statistics: ***$p <$ 0.001, one-way Tukey's ANOVA analysis, comparisons with healthy condition. Error bars indicate SEM. ***D***, Surface area of degenerating, but not healthy, axon bundles decreases over time when cocultured with rat microglia. The numbers represent quantification of percentage clearance of axon debris. ***E***, Confocal microscopy demonstrates engulfment (left panel) and uptake (right panel; orthogonal analysis) of degenerating TdTomato-labeled axons (red) by two microglial cells (green, Iba1).

column white matter tracts, all IBA1+ cells were identified, and colocalization with SMI31/32 and Lamp1 was determined for each cell by orthogonal analysis. A total of 8–10 35 μm sections was examined per mouse, and four mice were analyzed per group; since, on average, we counted >40 microglia per section, >1200 microglia were counted per condition. Counting was performed in blinded fashion and independently reproduced by two independent individuals. Although anatomical position varied slightly between sections, the overall distribution of sections analyzed was similar in each animal.

For gene expression analysis in microglia following dorsal root axotomy, microglia were isolated and analyzed *ex vivo* at various time points after axotomy. Mice were perfused with cold HBSS, spinal cords were isolated, and microglia/macrophages were separated at the 70–37% interphase using a Percoll gradient (GE Healthcare) as previously described (Cardona et al., 2006). Microglia/macrophages were further purified by passing through a MACS cell separator column with CD11b beads (MACS; Miltenyi Biotec), resulting in >95% CD11b-positive cells as determined by FACS. RNA isolation, cDNA preparation, and real-time PCR were performed as described above.

Results

Development of a microfluidic system to study microglial phagocytosis of degenerating axons

We used micropatterning of PDL (Fig. 1*Ai*) in combination with existing microfluidic technologies (Fig. 1*Aii*) to create a novel platform to spatially and fluidically isolate micrometer-scale (25 μm) axon bundles from neuronal cell bodies (Fig. 1*Aiii*). The patterning of axon bundles allowed clear visual demarcation of regions in which axonal surface area could be reproducibly quantified, a metric that was critical for assessment of axon debris clearance. Addition of NO donor specifically to the neuronal cell bodies resulted in a reduction in the number of extending growth cones, followed by focal swellings along the axon, and culminated in axon disintegration and accumulation of axonal debris. Morphologic changes within axons typically began to be detectable within 8 h of addition of NO donor. Notably, once axonal debris was generated, it remained stationary throughout the time course of the experiment as evidenced in Figure 1*B*. Under the experimental conditions, no nitrites were detected on the axon side, confirming fluidic isolation of the devices and suggesting that the axons were undergoing degeneration as a result of selective injury to neuronal cell bodies. In addition to morphologic changes indicative of axon degeneration, intra-axonal ATP also decreased following application of NO to cell bodies. ATP levels decreased to 50% within 2 h and were nearly undetectable by 16 h (Fig. 1*C*). Thus, both morphological and biochemical methods confirm progressive axonal degeneration following NO application specifically to neuronal cell bodies.

To study interactions between microglia and degenerating axons, we cocultured microglia on the axonal side of our devices (Fig. 1*Aiv*). Microglia cocultured with healthy axons continually extended processes and made brief but frequent contacts with axons without perturbing the overall appearance of the axonal bundle (Fig. 1*D*). However, microglia cocultured with degenerating axons were seen clearing axonal debris (Fig. 1*D*) in a time-dependent manner. Quantification of axonal bundle surface area

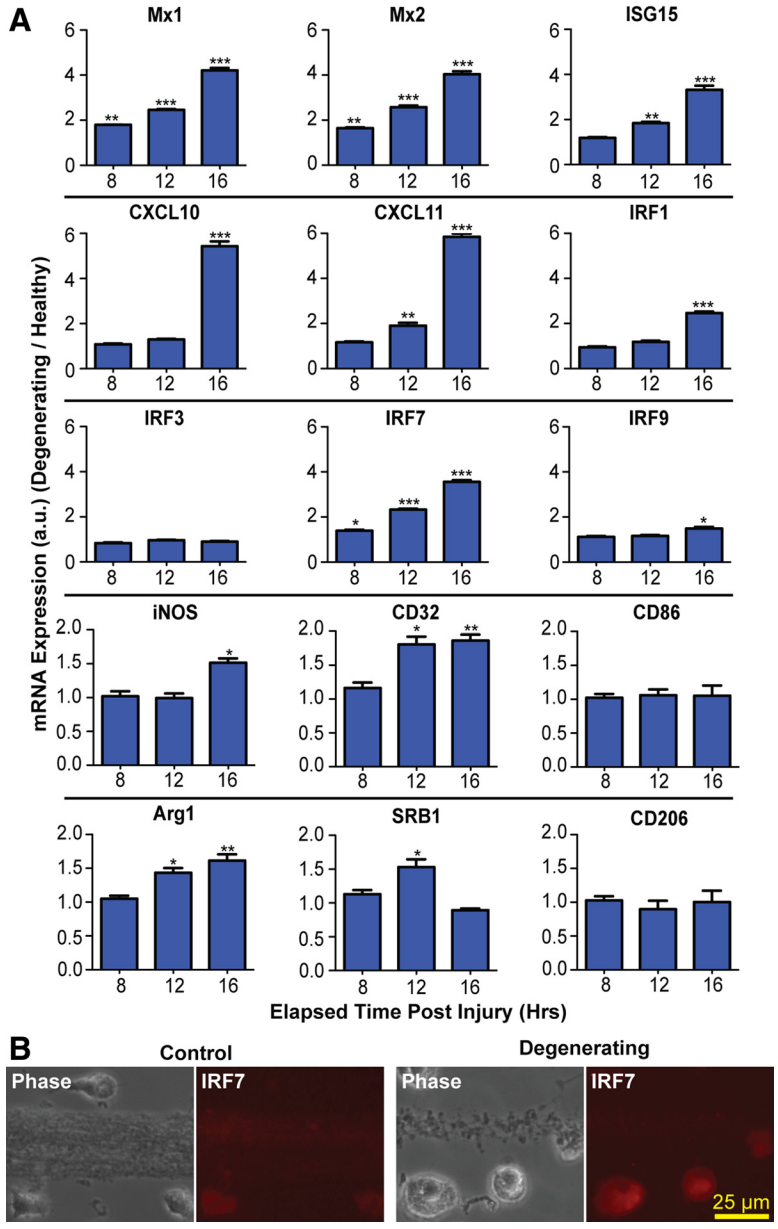

Figure 2. Axon degeneration induces type-1 IFN genes in microglia. ***A***, Real-time PCR shows induction of ISGs and IRFs in rat microglia cocultured with degenerating axons. All values are normalized to β-actin. Statistics: Student's *t* test, degenerating versus control at each time point. $^{*}p < 0.05$; $^{**}p < 0.01$; $^{***}p < 0.001$. Error bars indicate SEM. ***B***, Immunostaining with antibody to IRF7 at 24 h.

as a function of time revealed that the bundle area of healthy axons either remained unchanged or grew slightly due to continued axon outgrowth. However, in the setting of axonal degeneration, microglia phagocytosed axonal material in a time-dependent fashion, clearing up to 40% of the bundle area within the 16 h experimental window (Fig. 1*D*). Furthermore, confocal microscopy confirmed the internalization of fluorescently labeled axon debris fragments (red) within microglia (Fig. 1*E*).

Genes associated with type-1 IFNs are upregulated in microglia cocultured with degenerating axons

Having established the time course of axon degeneration and phagocytosis in our microfluidic system, we next performed a comparative microarray analysis of microglia cocultured with healthy versus degenerating axons. The microarray data revealed upregulation of many genes associated with type-1 IFN signaling in response to axon degeneration (data not shown). We used quantitative PCR to confirm upregulation of key interferon-stimulated genes (ISGs), including Mx1, Mx2, and ISG15 as well as the interferon-stimulated chemokines CXCL10 and CXCL11. In addition, several interferon response factors (IRFs), including IRF1, IRF7, and IRF9, were upregulated following axon degeneration (Fig. 2*A*). The time course of induction of these type-1 IFN genes paralleled the course of axonal degeneration and phagocytosis that we observed by time-lapse microscopy (Fig. 1*D*). IRF3 levels did not differ between healthy and degenerating conditions, consistent with previous reports of constitutive expression of this transcription factor during microglial activation (Izaguirre et al., 2003; Noppert et al., 2007). To further examine the activation state of the microglia in our coculture system, we analyzed the expression of genes associated with classical (M1) and alternate (M2) activation states. We found that several M1 (iNOS, CD32) and M2 (Arg1, SRB1) genes were rapidly upregulated after axon degeneration, while expression levels of the M1 gene CD86 and the M2 gene CD206 were unchanged (Fig. 2*A*). These data parallel the acute changes in microglial gene expression observed *in vivo* following spinal cord injury (Kigerl et al., 2009).

Since the pool of RNA used for microarray experiments was composed of a small amount of axonal RNA in addition to microglial RNA, it was conceivable that changes in axonal expression contributed to our findings. Therefore, we next sought to determine whether the type-1 IFN pathway was induced in microglia or in axons. Immunocytochemistry with an antibody to IRF7, a master regulator of type-1 IFN signaling (Honda et al., 2005), demonstrated that IRF7 immunoreactivity was upregulated in microglia cocultured with degenerating axons, and was not observed in axons (Fig. 2*B*). Finally, we asked whether upregulation of the type-1 IFN response occurs as a general response to microglial phagocytosis. IRF7 expression was quantified after addition of either microbeads or HEK 293 cell debris to microglia. Although microglia were observed to phagocytose microbeads and HEK debris, the level of IRF7 expression was not increased (data not shown).

TRIF inhibition blocks microglial phagocytosis of axons

We next investigated the molecular mechanisms of axonal debris clearance by microglia. Based on our data that showed an upregulation of genes associated with type-1 IFN signaling, we hypothesized that microglia may use TLRs to recognize and initiate the clearance of axon debris. Since most TLRs mediate their cellular effects through the adapter molecule MyD88, we initially used a

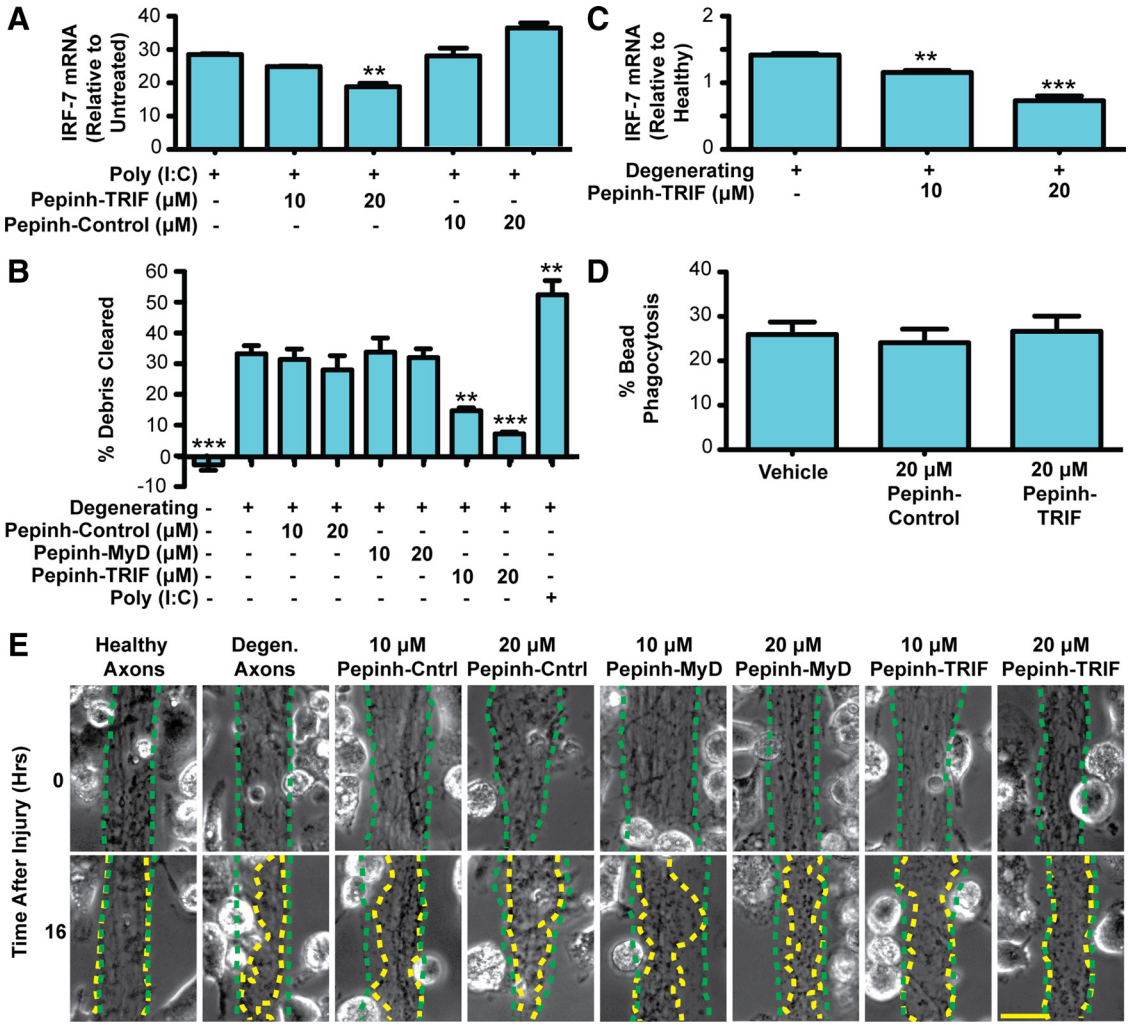

Figure 3. Axonal debris is cleared by microglia in a TRIF-dependent manner. ***A***, Rat microglia were preincubated with peptide inhibitors, followed by treatment with poly(I:C). Real-time PCR of IRF7 shows that TRIF inhibition by Pepinh-TRIF decreases IRF7 expression at 16 h. ***B***, Quantification of axon debris clearance at 16 h demonstrates that TRIF inhibition markedly reduces axon debris clearance in a dose-dependent manner. One-way Tukey's ANOVA analysis, comparisons with degenerating condition; *F* value, 18.31. ***C***, Real-time PCR of microglia cocultured with degenerating axons demonstrates that TRIF inhibition results in decreased IRF7 expression. ***D***, TRIF inhibition does not alter bead phagocytosis. A total of 1×10^6 FluoSpheres was added to microglia in 96-well plates. The percentage of microglia that took up more than one bead was determined. Error bars indicate SEM. $^{**}p < 0.01$; $^{***}p < 0.001$. ***E***, Representative images of debris clearance. The dotted green traces outline axon bundle areas at time 0, and the dotted yellow traces outline the axon bundles after 16 h. Scale bar, 25 μm.

well characterized peptide inhibitor of MyD88 signaling (Loiarro et al., 2005; Toshchakov et al., 2005). To confirm optimal concentrations of the peptide blocker, we pretreated microglia with varying blocker concentrations followed by stimulation with LPS, which is known to exert effects through MyD88. Peptide concentrations of 10 and 20 μM resulted in significant reductions in production of LPS-induced NO without affecting microglial viability (data not shown). However, no effect was found on clearance of axonal debris (Fig. 3*B*).

Next, we used a peptide blocker of TRIF signaling (Toshchakov et al., 2005). The optimum concentration of this peptide was confirmed by stimulating microglia with the TLR3 agonist poly(I:C), whose effects are mediated through TRIF. At the concentrations tested, we found that the TRIF blocker reduced poly(I:C)-induced IRF7 expression in a dose-dependent manner without affecting cell viability (Fig. 3*A*). Application of the TRIF blocker to the microglial/axon compartment of our microfluidic coculture platform resulted in significant reduction in clearance (Fig. 3*B*,*E*), while uptake of microbeads was not affected by the blocker (Fig. 3*D*). In addition, the attenuation in axonal debris clearance through blockade of TRIF activity was accompanied by reductions in IRF7 expression (Fig. 3*C*). Interestingly, the addition of poly(I:C) to microglia cocultured with degenerating axons resulted in a further increase in axon debris clearance (Fig. 3*B*).

p38 MAPK is involved in microglial clearance of axon debris

TRIF-mediated signaling has been shown to activate the p38 MAPK pathway (O'Neill and Bowie, 2007), and microglial p38 MAPK has been implicated in phagocytosis (Doyle et al., 2004). We first determined whether the p38 MAPK cascade was activated in microglia exposed to degenerating axons. Western blotting demonstrated that degenerating axons induce phosphorylation of p38 MAPK in our microglia–axon coculture system (Fig. 4*A*). We next used the p38 MAPK-specific inhibitor SB203580 to assess for a functional role of the p38 MAPK cascade in microglial phagocytosis of degenerating axons. Addition of SB203580 resulted in a reduction of axon debris clearance (Fig. 4*B*) without impacting microglial viability (data not shown). Notably, inhibition of p38 MAPK did not impact the course of axon

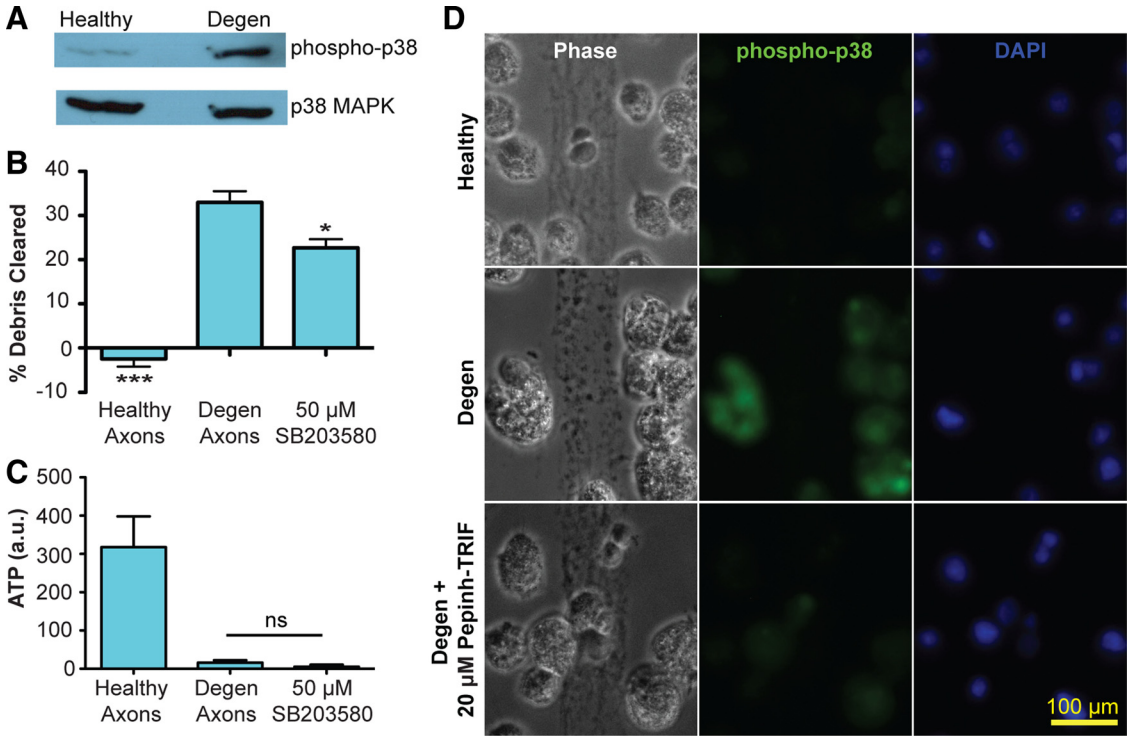

Figure 4. p38 MAPK mediates axon debris clearance. Rat microglia were cocultured with either healthy or degenerating axons for 16 h. ***A***, Representative Western blotting showed increase of phospho-p38 in microglia in the setting of axonal degeneration. Total p38 MAPK was unchanged. ***B***, Axonal debris clearance by microglia was reduced by SB203580, a p38 inhibitor. Data for healthy and degenerating conditions are taken from Figure 3, as these experiments were performed together. One-way Tukey's ANOVA analysis, comparisons with degenerating axons; *F* value, 40.87. $^{*}p < 0.05$; $^{***}p < 0.001$. ***C***, Addition of SB203580 did not affect axon degeneration, as measured by changes in intra-axonal ATP levels at 16 h. Error bars indicate SEM. ***D***, Immunostaining with antibody to phospho-p38 shows decreased immunoreactivity after TRIF inhibition.

degeneration, as measured by morphological changes (data not shown) or intra-axonal ATP measures (Fig. 4*C*). These data implicate p38 MAPK signaling in microglial phagocytosis of axons. To confirm that the p38 MAPK cascade was activated in microglia, rather than axons, following axon degeneration, we performed immunocytochemistry using a phospho-p38 antibody. We found that phospho-p38 immunoreactivity appeared in microglia exposed to degenerating, but not healthy, axons (Fig. 4*D*). Furthermore, addition of the TRIF blocking peptide reduced the level of phospho-p38 labeling in microglia exposed to degenerating axons, suggesting that TRIF activation is upstream of microglial p38 MAPK signaling in the setting of axonal degeneration.

Microglia derived from TRIF knock-out mice exhibit impaired phagocytosis of axonal debris

We next confirmed the role of TRIF signaling in axonal phagocytosis using microglia derived from both wt and TRIF KO mice. Healthy and degenerating axons were cocultured with both wt and TRIF KO microglia. Under the setting of axonal degeneration, wt mice robustly cleared axonal debris (Fig. 5*A*). However, we found that clearance of axonal debris by TRIF KO microglia was significantly lower than wt counterparts (Fig. 5*A*,*B*). We next sought to determine whether the TRIF pathway is involved in axon debris phagocytosis by macrophages, which are also likely to be present in the CNS during neurodegeneration and neuroinflammation. Peritoneal macrophages were isolated from wt and TRIF KO mice and cocultured with degenerating axons. We found that TRIF deficiency resulted in a marked decrease in axon debris clearance by macrophages (WT clearance, 56.5 ± 5.8%; TRIF KO clearance, 15.0 ± 3.3%). Thus, both pharmacological and genetic approaches demonstrate that TRIF signaling plays an important role in microglial/macrophage clearance of axonal debris.

Phagocytosis following axotomy is decreased in TRIF KO microglia

In previous experiments, axon degeneration was initiated by addition of NO donor to the cell body side. Although we found no evidence of NO diffusion to the axonal/microglial side of our chambers, we wanted to address the possibility that minute, undetectable amounts of NO influenced the microglial response. Therefore, we sought to develop a system in which we could induce axon degeneration in the absence of exogenous chemicals. We modified our device to have an unrestricted access port, thereby allowing us to mechanically cut axon bundles to model axotomy-induced axonal degeneration (Fig. 6*A*). Microglia were seeded within the middle compartment immediately following axotomy, and time-lapse microscopy was used to capture the microglial response. We found that wt mouse microglia rapidly cleared axon debris following axotomy (Fig. 6*B*). Clearance was faster than with NO-mediated axonal degeneration, likely due to the more rapid degenerative events following cutting compared with chemical injury.

We then examined the capacity of TRIF KO microglia to clear axotomy-derived axon debris. When cocultured with healthy axons, TRIF KO microglia behaved similarly to wt microglia, in that they remained very mobile and continually traversed along axon bundle tracks, making brief but intimate contacts (data not shown). However, in the setting of axotomy, TRIF KO microglia were less able to efficiently clear axonal debris compared with their wt counterparts (Fig. 6*B*). In general, the TRIF KO microglia exhibited slightly slower migration toward axonal debris, fol-

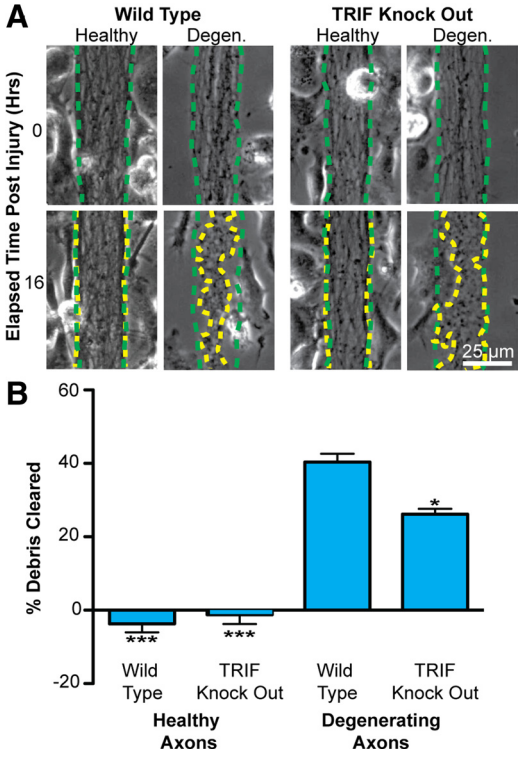

Figure 5. Axonal debris clearance is attenuated in microglia derived from TRIF-knock-out mice. ***A***, Microglia derived from wt and TRIF KO mice were cocultured with healthy or degenerating axons for 16 h. An identical experiment setup as in Figure 3 was used to quantify the extent of axon debris clearance by microglia. The dotted green traces outline axon bundle areas at time 0, whereas the dotted yellow traces outline the same region after 16 h. ***B***, Quantification of axon debris clearance revealed a reduced clearance capacity for TRIF KO microglia compared with wt counterparts. One-way Tukey's ANOVA analysis, comparisons with WT degenerating condition; *F* value, 59.02. $*p < 0.05$; $***p < 0.001$. Error bars indicate SEM.

lowed by a reduced capacity to engulf material, culminating in the microglia circling about a mass of axonal debris.

TRIF deficiency blocks phagocytosis of axons in adult mice *in vivo*

We next examined whether TRIF plays a role in mediating clearance of degenerating axons in adult mice. We induced CNS axon degeneration by lumbar dorsal root axotomy, which results in rapid Wallerian degeneration of sensory axons in the dorsal columns, with relative sparing of myelin (George et al., 1995; Zhang et al., 2009). We first determined whether dorsal root axotomy results in induction of the type-1 interferon response in microglia. *Ex vivo* isolated spinal cord microglia were subjected to real-time PCR at several time points following dorsal root axotomy (Fig. 7*A*,*B*). We found that both IRF7 and CXCL10 expression are induced in microglia following axotomy; similar to our *in vitro* findings, IRF7 expression is induced earlier than CXCL10. We next performed immunohistochemistry to examine axonal phagocytosis *in vivo*. In wt and TRIF KO animals, microglial density in the dorsal columns was similar (data not shown), and microglia accumulated in the injured dorsal column within 2 d following axotomy (Fig. 7*C*). Axonal phagocytosis was then quantified by assessing the percentage of microglia that had taken up axonal material. We found colocalization of SMI^+ axons and $Lamp1^+$ endosomes within $Iba1^+$ microglia in the injured dorsal column 2 d after axotomy (Fig. 7*D*). Colocalization of these markers was not observed on the noninjured side. Quantification of axonal phagocytosis demonstrated 6.8 ± 0.6% of microglia actively phagocytosing axons on the injured side in wt animals. In TRIF KO animals, only 4.6 ± 0.3% of microglia were found to be actively phagocytosing axons, representing a 32% decrease compared with wt (Fig. 7*E*). To determine whether a comparable decrease in phagocytosis occurs *in vitro*, we cocultured wt or TRIF KO microglia with TdTomato-labeled axons, and then induced axon degeneration. Using confocal microscopy, we found a similar decrease in the percentage of TRIF microglia phagocytosing axonal debris (Fig. 7*F*).

Microglial clearance of axon debris facilitates axon outgrowth

To further determine the significance of axon debris clearance by microglia, we explored its role in axon outgrowth. To test whether the accumulation of unmyelinated axonal debris from degenerating CNS axons affects outgrowth of new axons, we collected unmyelinated axonal debris from our microfluidic devices following axotomy. After collection, we added the debris to the axonal compartment of new devices, and tracked outgrowth of healthy axons into this compartment. We found that the presence of axonal debris in the field of newly growing axons markedly inhibited outgrowth of these axons, compared with control compartments in which no debris or non-neuronal debris was present (Fig. 8*A*,*B*). Axon growth rates were found to be normal until the growing axon encountered axonal debris, at which point overall growth rates declined markedly (Fig. 8*C*). Quantification of growth rates of individual axons in the 2 h following contact with axon debris revealed that 30% of axons retracted, 24% either stopped growing or exhibited reduced growth (≤ 5 μm/h), and 46% continued to grow at a rate of >5 μm/h. Next, we asked whether TRIF-mediated microglial clearance of axonal debris affects outgrowth of new axons. We examined the growth of new axons into fields of axonal debris cocultured with either wt or TRIF KO microglia (Fig. 8*D*). To distinguish growing axons from microglial processes in this coculture paradigm, immunostaining for β-III-tubulin was performed and the longest axon in each bundle was quantified. We found that axon outgrowth into fields of axonal debris was diminished in the presence of TRIF KO microglia compared with wt microglia (Fig. 8*E*,*F*). Notably, this reduction in axon outgrowth was dependent upon the presence of axonal debris, since axon outgrowth in the absence of axonal debris was unaffected by TRIF KO microglia. Together, these data suggest that TRIF-dependent removal of debris by microglia facilitates axon outgrowth.

Discussion

Using a novel microfluidic platform that enables coculture of microglia with CNS axons, we demonstrate that TRIF plays an important role in microglial clearance of degenerating axons. Mechanistically, axon degeneration results in the induction of type-1 IFN genes within microglia. Pharmacologic and genetic disruption of TRIF signaling blocks induction of the interferon response and inhibits microglial phagocytosis of axon debris. Furthermore, phosphorylation of p38 MAPK is a signaling component downstream of TRIF in microglia cocultured with degenerating axons, and inhibition of p38 MAPK also inhibited clearance of axon debris. Importantly, we demonstrate impaired axonal outgrowth in the presence of unmyelinated axonal debris and enhanced axonal outgrowth following its removal by microglia. Overall, we provide evidence that TRIF-mediated signaling plays a critical role in axonal debris clearance by microglia, thereby facilitating a more permissive environment for axonal outgrowth.

The precise spatial and temporal control of microenvironments achievable by microfluidic devices has positioned them as

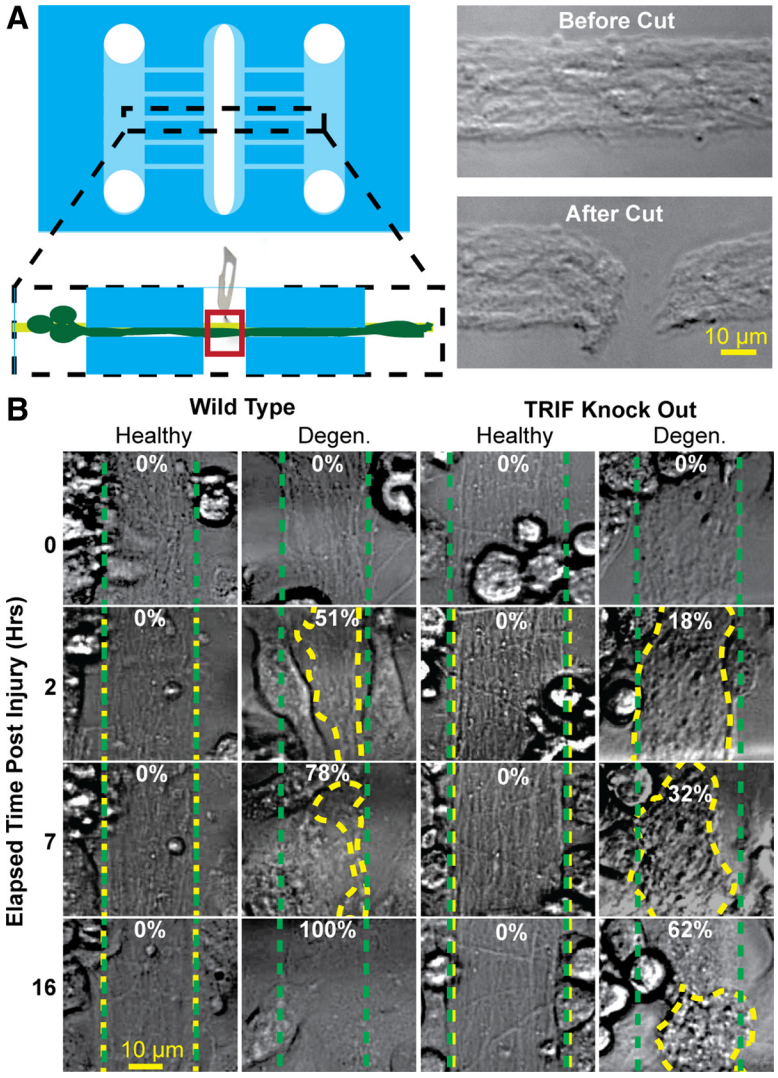

Figure 6. Microglia clear axonal debris following axotomy. ***A***, The microfluidic platform was modified by creation of a third compartment. Before addition of wt or TRIF KO mouse microglia, a scalpel was used to sever a 10–20 μm segment of the bundle, thereby inducing axon degeneration to distal axon segments. ***B***, Mouse microglia were then cocultured with either healthy or cut axon bundles to assess the extent of axon debris clearance. The dotted green traces outline axon bundle areas at time 0, and the dotted yellow traces outline the axon bundles after indicated times. The numbers refer to the percentage clearance of degenerating axons.

important tools for the study of various aspects of neuronal behavior, including neuronal and axonal growth, synapse formation, neuropharmacology, and electrophysiology (Wang et al., 2009; Taylor and Jeon, 2010). Our platform uniquely used a combination of micropatterning and mechanical guidance to allow primary microglia to intimately interact with bundles of CNS axons. The resulting robust, reproducible model of microglial phagocytosis of axonal debris enabled a detailed investigation of the molecular mechanisms controlling phagocytosis and identified TRIF as a mediator of axon debris clearance. Importantly, these findings were applicable *in vivo*, highlighting the potential utility of this platform to extend our knowledge of microglial–axon interactions.

Our microarray-derived gene expression analysis of purified microglia cocultured with axons indicated that type-1 IFN pathways were induced in microglia phagocytosing degenerating axons. Type-1 IFNs, originally identified by their antiviral activity, are now known to mediate a broad range of biological functions, often in a cell type-specific manner (Noppert et al., 2007). Importantly, recent evidence suggests that type-1 IFN signaling in multiple cell types can regulate responses to sterile CNS injury and neurodegeneration. For example, mice deficient in type-1 IFN signaling develop more severe experimental autoimmune encephalomyelitis (EAE) (Teige et al., 2004), suggesting a role in the control of inflammation-induced injury. IFN signaling pathways have also recently been found to be upregulated in spinal cord astrocytes in an amyotrophic lateral sclerosis mouse model. In these mice, deletion of the IFN receptor resulted in prolongation of survival (Wang et al., 2011). In addition, one report demonstrated that sterile axon injury caused by entorhinal axotomy also induces type-1 IFN signaling *in vivo* (Khorooshi and Owens, 2010). Our data support this finding of upregulation of microglial type-1 IFN responses following axon injury, and underscore that our microfluidic system recapitulates features of the *in vivo* microglial response to axon degeneration. Notably, in our platform, microglia are selectively cultured with unmyelinated axons, implying that degenerating axons can directly signal to microglia to upregulate the type-1 IFN response in the absence of myelin, neurons, or other glial cells.

We found that expression of IRF1, IRF7, and IRF9 were increased upon axonal degeneration, while IRF3 RNA levels remained unchanged. Similar findings have been noted in the setting of microbial infection (Perry et al., 2005). Following exposure of cells to viral or bacterial components, IRF3 expression remains unchanged (Izaguirre et al., 2003; Noppert et al., 2007). However, IRF3 has been found to play a key role in the induction of the IFN response, as it becomes phosphorylated, translocates into the nucleus, and promotes expression of IFN-β (Malmgaard, 2004). IRF3-induced IFN-β production, in turn, induces expression of IRF7, which can then act as a master transcriptional regulator of a large number of type-1 IFN genes (Honda et al., 2005). Thus, the patterns of IRF expression that we observed in microglia following axon degeneration parallel those seen in responses to foreign pathogens.

Type-1 IFN responses can be triggered via TLR-dependent and TLR-independent pathways. The TLRs are a family of pattern recognition receptors that recognize viral and bacterial products and signal through at least five TIR domain-containing adapter proteins, including MyD88 and TRIF (Pålsson-McDermott and O'Neill, 2007). MyD88 signaling is used by nearly all TLRs except TLR3, resulting in induction of NF-κB, often leading to the production of inflammatory cytokines and chemokines. TRIF mediates signaling through TLR3 and TLR4, and recent evidence also suggests a role in TLR5-dependent pathways (Choi et al., 2010). Downstream of TLR3 and TLR4, TRIF activation of the IRF3/7 pathway leads to secretion of type-1

IFNs (α/β) (Yamamoto et al., 2002a,b, 2003; Han et al., 2004; Hasan et al., 2007). We found that pharmacological blockade and genetic deletion of TRIF impaired axonal debris clearance, while use of the TLR3 agonist poly(I:C), which activates TRIF signaling, resulted in increased debris clearance. These data indicate that TRIF-mediated signaling plays an important role in axonal debris clearance by microglia and suggest the involvement of TLRs in axon debris clearance.

TRIF activation results in propagation of several downstream signaling cascades including NF-κB and MAPKs (Pålsson-McDermott and O'Neill, 2007; Cekic et al., 2009; Gais et al., 2010). p38 MAPK has been previously implicated in phagocytosis of microbes (Blander and Medzhitov, 2004; Doyle et al., 2004) and fibrillar β-amyloid (Reed-Geaghan et al., 2009). Potential mechanisms by which p38 MAPK signaling can influence phagocytosis include directing endocytic traffic by regulating the activity of GDI (guanyl-nucleotide dissociation inhibitor) on Rab proteins (Cavalli et al., 2001) and influencing membrane ruffling and engulfment via effects on the Rho GTPase Rac1 (Zuluaga et al., 2007). We found that TRIF directs activation of p38 MAPK activity, and that p38 MAPK signaling mediates clearance of axonal debris. A role for microglial p38 MAPK signaling during engulfment of axonal debris has been recently described using a cortical explant model (Tanaka et al., 2009). Interestingly, in that study, primary microglia were only found to phagocytose axonal debris and activate p38 MAPK in the presence of LPS. Since LPS, a TLR4 agonist, can itself induce activation of p38 MAPK in microglia (Bachstetter et al., 2011), the contribution of axonal debris to the induction of p38 MAPK remained unclear in that setting. In contrast, in our experimental paradigm in which microglia freely traversed between bundles of axons, primary microglia phagocytosed degenerating axons in the absence of LPS, and this phagocytosis was dependent upon activation of p38 MAPK. Overall, our data suggest the p38 MAPK cascade as a common downstream pathway used by phagocytes for removal of both microbes and cellular debris.

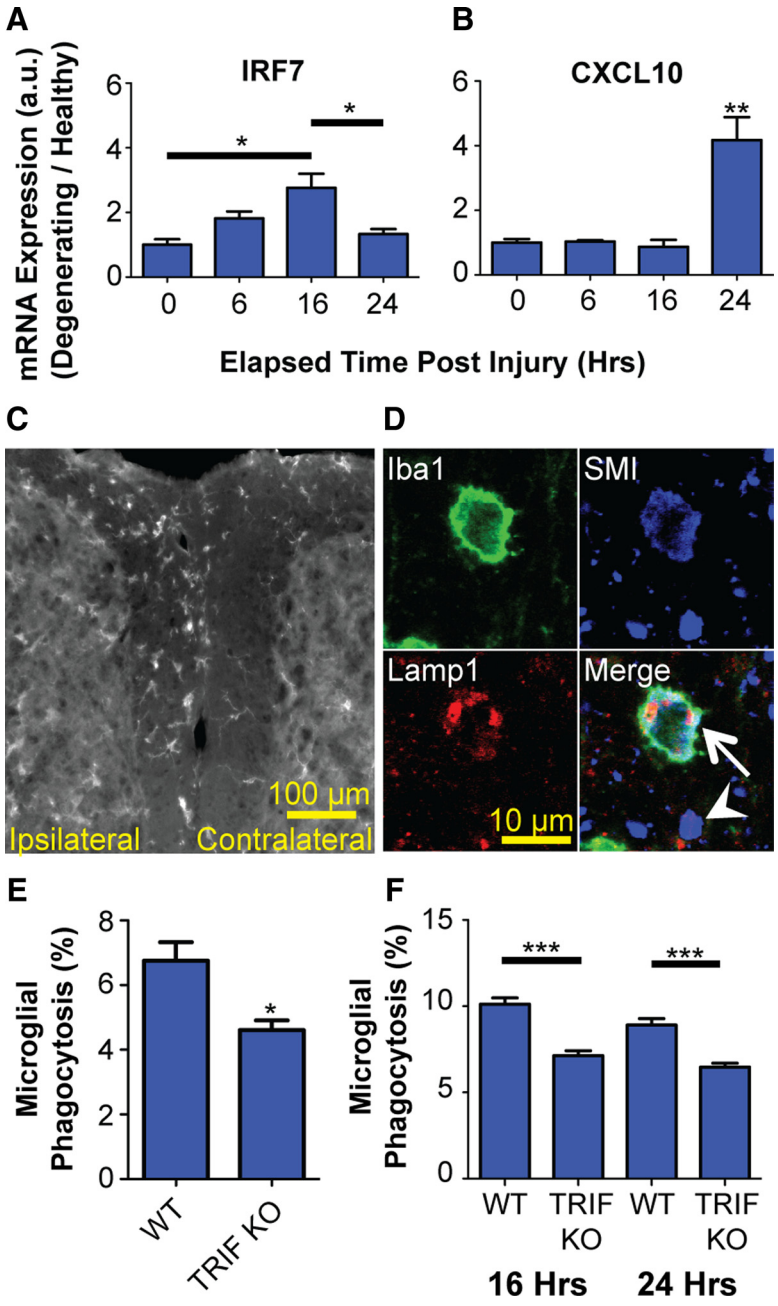

Figure 7. TRIF KO impairs microglial phagocytosis *in vivo*. Real-time PCR of *ex vivo* isolated microglia following dorsal root axotomy demonstrates induction of IRF7 (Tukey's ANOVA; *F* value, 7.95) (***A***) and CXCL10 (Tukey's ANOVA; $^{**}p < 0.01$ compared with no axotomy control, labeled "0"; *F* value, 18.16) (***B***). ***C***, Dorsal root axotomy results in microglial accumulation in ipsilateral dorsal column within 2 d of injury. Scale bar, 100 μm. ***D***, Triple-label immunohistochemistry and confocal microscopy of ipsilateral side show neurofilament-positive axons (SMI) colocalized with endosomes (Lamp1) within microglia (Iba1). Arrow, Microglia phagocytosing axon; arrowhead, extracellular (nonphagocytosed) axonal material. Scale bar, 10 μm. ***E***, Quantification of axon phagocytosis by microglia ($Iba1^+$ SMI^+ cells) in ipsilateral dorsal columns at 2 d following axotomy. $^*p < 0.05$, Student's *t* test. ***F***, *In vitro* quantification of axon phagocytosis by wt or TRIF KO microglia cocultured with TdTomato-labeled axons. $^{***}p < 0.001$, Tukey's ANOVA analysis; *F* value, 28.23. Error bars indicate SEM.

The phagocytic clearance of dying cells during development and in neurodegenerative diseases is generally considered beneficial (Napoli and Neumann, 2009). In the developing brain of *Drosophila*, phagocytic glial cells have been shown to engulf axonal varicosities during axonal pruning (Awasaki and Ito, 2004; Awasaki et al., 2006). In the developing murine CNS, the microglia complement receptor C3 has been implicated in removal of unwanted synapses (Stevens et al., 2007). In acute CNS injury, too, phagocytosis of endogenous cells and their components may play a crucial role in repair. Indeed, insufficient removal of myelin debris by phagocytes may contribute to the failure of axonal regeneration (David and Lacroix, 2003; Vargas and Barres, 2007). Transplantation of myeloid cells transduced with TREM2 to enhance phagocytosis resulted in reduced injury and improved recovery from EAE (Fenoglio et al., 2007) (Takahashi et al., 2007). Since myelin is known to contain several growth inhibitory mol-

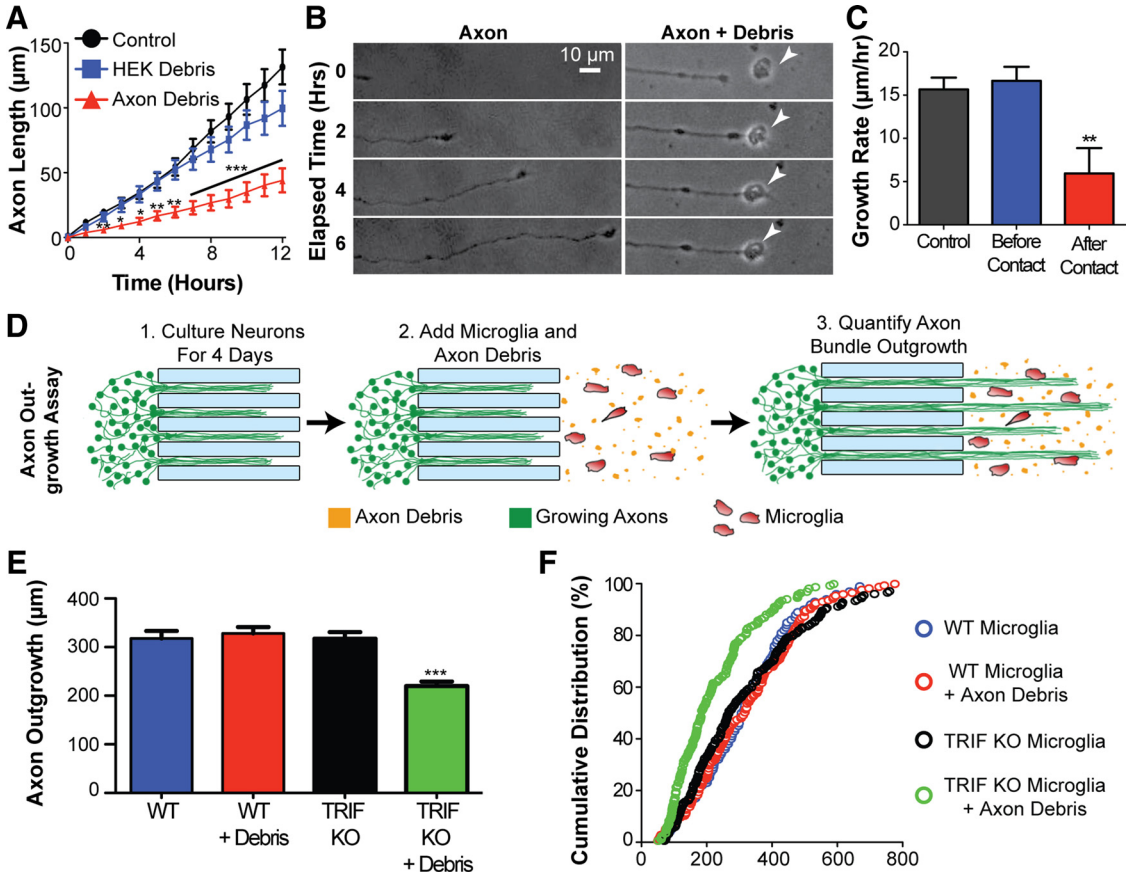

Figure 8. TRIF-dependent microglial clearance of axon debris facilitates axon outgrowth. ***A***, Quantification of axon outgrowth was performed in the presence of axonal debris, HEK cell membrane debris, or neither (control). Axonal debris inhibited axon outgrowth compared with control (no debris), while no significant difference was observed with HEK debris. ANOVA, Tukey's posttest. ***B***, Representative time-lapse images showing impaired axon outgrowth upon contact with axon debris (arrowhead) (***C***). Quantification of axon outgrowth in the 2 h before (Before Contact) and following (After Contact) contact with axon debris. Control refers to no axon debris present. n = minimum of 20 axons per condition; axons interacting with multiple particles of debris were excluded from this analysis. $^{**}p < 0.01$, After Contact compared with either of the two other conditions; ANOVA, Tukey's posttest; F value, 8.017. ***D***, Schematic of the axon outgrowth experiments in ***E*** and ***F***. ***E***, ***F***, Axonal outgrowth into fields of microglia (either WT or TRIF KO) cocultured with axonal debris is quantified and represented by bar graph and by cumulative distribution. $^{***}p < 0.01$, ANOVA, Tukey's posttest; F value, 16.58. Error bars indicate SEM.

ecules (David and Lacroix, 2003), enhanced regeneration following its removal is perhaps not surprising. Here, we provide evidence that unmyelinated axonal debris impairs outgrowth of new axons and we find that clearance of axon debris by microglia facilitates outgrowth of new axons. Importantly, in the presence of TRIF KO microglia, axon debris is not cleared as efficiently and outgrowth of new axons is impaired. Our data support a single previous report that shows enhanced axonal regrowth following axon debris clearance by microglia (Tanaka et al., 2009) and reveal the importance of the microglial TRIF pathway in creating a permissive environment for axon regrowth following injury. Since many axons in white matter tracts are unmyelinated, clearance of axonal debris, in addition to clearance of myelin, may play an important role in CNS regeneration.

In recent years, several endogenous ligands of TLRs that mediate activation of innate immunity have been identified (Okamura et al., 2001; Karikó et al., 2004; Park et al., 2004; Kim et al., 2006; Imai et al., 2008). In the CNS, microglial TLR signaling has been shown to be triggered by endogenous signals released from injured neurons (Kim et al., 2006; Pais et al., 2008; Stewart et al., 2010). In peripheral macrophages, TLR3 has been demonstrated to be a sensor of endogenous tissue necrosis in the absence of viral activation (Cavassani et al., 2008). Presently, we do not know the axon-derived ligands responsible for the activation of TRIF-mediated signaling and subsequent axonal debris clearance by microglia. Preliminary studies indicate that components of the degenerating axon membrane alone can trigger low levels of microglial clearance, and that higher efficiencies of axon debris clearance may require additional soluble factors derived from degenerating axons (M. A. Tegenge and A. Venkatesan, unpublished observations).

The observation that TRIF mediates clearance of degenerating axons by microglia has several important implications. Modulation of TRIF activity may serve as a new therapeutic approach to promote axon debris clearance and enhance CNS regeneration following axonal degeneration. Such approaches may be particularly important given the evidence in EAE and in MS that axonal injury occurs early, may precede demyelination, and occurs chronically. Perhaps more importantly, many antagonists to TLR/TRIF pathways are currently in clinical development as potential therapeutics for inflammatory and autoimmune conditions (Kanzler et al., 2007). Our findings suggest that the circumstances and timing of such antagonism following CNS injury may need to be carefully considered, as unintended consequences on processes such as axonal debris clearance and regeneration may counterbalance therapeutic effects.

References

Awasaki T, Ito K (2004) Engulfing action of glial cells is required for programmed axon pruning during *Drosophila* metamorphosis. Curr Biol 14:668–677.

Awasaki T, Tatsumi R, Takahashi K, Arai K, Nakanishi Y, Ueda R, Ito K (2006) Essential role of the apoptotic cell engulfment genes draper and ced-6 in programmed axon pruning during *Drosophila* metamorphosis. Neuron 50:855–867.

Bachstetter AD, Xing B, de Almeida L, Dimayuga ER, Watterson DM, Van Eldik LJ (2011) Microglial p38alpha MAPK is a key regulator of proinflammatory cytokine up-regulation induced by Toll-like receptor (TLR) ligands or beta-amyloid (Abeta). J Neuroinflammation 8:79.

Bignami A, Dahl D, Nguyen BT, Crosby CJ (1981) The fate of axonal debris in Wallerian degeneration of rat optic and sciatic nerves. Electron microscopy and immunofluorescence studies with neurofilament antisera. J Neuropathol Exp Neurol 40:537–550.

Blander JM, Medzhitov R (2004) Regulation of phagosome maturation by signals from Toll-like receptors. Science 304:1014–1018.

Cardona AE, Huang D, Sasse ME, Ransohoff RM (2006) Isolation of murine microglial cells for RNA analysis or flow cytometry. Nat Protoc 1:1947–1951.

Cavalli V, Vilbois F, Corti M, Marcote MJ, Tamura K, Karin M, Arkinstall S, Gruenberg J (2001) The stress-induced MAP kinase p38 regulates endocytic trafficking via the GDI:Rab5 complex. Mol Cell 7:421–432.

Cavassani KA, Ishii M, Wen H, Schaller MA, Lincoln PM, Lukacs NW, Hogaboam CM, Kunkel SL (2008) TLR3 is an endogenous sensor of tissue necrosis during acute inflammatory events. J Exp Med 205:2609–2621.

Cekic C, Casella CR, Eaves CA, Matsuzawa A, Ichijo H, Mitchell TC (2009) Selective activation of the p38 MAPK pathway by synthetic monophosphoryl lipid A. J Biol Chem 284:31982–31991.

Choi YJ, Im E, Chung HK, Pothoulakis C, Rhee SH (2010) TRIF mediates Toll-like receptor 5-induced signaling in intestinal epithelial cells. J Biol Chem 285:37570–37578.

Coleman M (2005) Axon degeneration mechanisms: commonality amid diversity. Nat Rev Neurosci 6:889–898.

David S, Lacroix S (2003) Molecular approaches to spinal cord repair. Annu Rev Neurosci 26:411–440.

Doyle SE, O'Connell RM, Miranda GA, Vaidya SA, Chow EK, Liu PT, Suzuki S, Suzuki N, Modlin RL, Yeh WC, Lane TF, Cheng G (2004) Toll-like receptors induce a phagocytic gene program through p38. J Exp Med 199:81–90.

Dubois-Dalcq M, Ffrench-Constant C, Franklin RJ (2005) Enhancing central nervous system remyelination in multiple sclerosis. Neuron 48:9–12.

Fadok VA, Bratton DL, Konowal A, Freed PW, Westcott JY, Henson PM (1998) Macrophages that have ingested apoptotic cells in vitro inhibit proinflammatory cytokine production through autocrine/paracrine mechanisms involving TGF-beta, PGE2, and PAF. J Clin Invest 101:890–898.

Fenoglio C, Galimberti D, Piccio L, Scalabrini D, Panina P, Buonsanti C, Venturelli E, Lovati C, Forloni G, Mariani C, Bresolin N, Scarpini E (2007) Absence of TREM2 polymorphisms in patients with Alzheimer's disease and frontotemporal lobar degeneration. Neurosci Lett 411:133–137.

Franklin RJ, Kotter MR (2008) The biology of CNS remyelination: the key to therapeutic advances. J Neurol 255 [Suppl 1]:19–25.

Gais P, Tiedje C, Altmayr F, Gaestel M, Weighardt H, Holzmann B (2010) TRIF signaling stimulates translation of TNF-α mRNA via prolonged activation of MK2. J Immunol 184:5842–5848.

George EB, Glass JD, Griffin JW (1995) Axotomy-induced axonal degeneration is mediated by calcium influx through ion-specific channels. J Neurosci 15:6445–6452.

George R, Griffin JW (1994) Delayed macrophage responses and myelin clearance during Wallerian degeneration in the central nervous system: the dorsal radiculotomy model. Exp Neurol 129:225–236.

Grommes C, Lee CY, Wilkinson BL, Jiang Q, Koenigsknecht-Talboo JL, Varnum B, Landreth GE (2008) Regulation of microglial phagocytosis and inflammatory gene expression by Gas6 acting on the Axl/Mer family of tyrosine kinases. J Neuroimmune Pharmacol 3:130–140.

Han KJ, Su X, Xu LG, Bin LH, Zhang J, Shu HB (2004) Mechanisms of the TRIF-induced interferon-stimulated response element and NF-κB activation and apoptosis pathways. J Biol Chem 279:15652–15661.

Hasan UA, Caux C, Perrot I, Doffin AC, Menetrier-Caux C, Trinchieri G, Tommasino M, Vlach J (2007) Cell proliferation and survival induced by Toll-like receptors is antagonized by type I IFNs. Proc Natl Acad Sci U S A 104:8047–8052.

Honda K, Yanai H, Negishi H, Asagiri M, Sato M, Mizutani T, Shimada N, Ohba Y, Takaoka A, Yoshida N, Taniguchi T (2005) IRF-7 is the master regulator of type-I interferon-dependent immune responses. Nature 434:772–777.

Hosmane S, Yang IH, Ruffin A, Thakor N, Venkatesan A (2010) Circular compartmentalized microfluidic platform: study of axon-glia interactions. Lab Chip 10:741–747.

Imai Y, Kuba K, Neely GG, Yaghubian-Malhami R, Perkmann T, van Loo G, Ermolaeva M, Veldhuizen R, Leung YH, Wang H, Liu H, Sun Y, Pasparakis M, Kopf M, Mech C, Bavari S, Peiris JS, Slutsky AS, Akira S, Hultqvist M, et al. (2008) Identification of oxidative stress and Toll-like receptor 4 signaling as a key pathway of acute lung injury. Cell 133:235–249.

Izaguirre A, Barnes BJ, Amrute S, Yeow WS, Megjugorac N, Dai J, Feng D, Chung E, Pitha PM, Fitzgerald-Bocarsly P (2003) Comparative analysis of IRF and IFN-alpha expression in human plasmacytoid and monocyte-derived dendritic cells. J Leukoc Biol 74:1125–1138.

Kanzler H, Barrat FJ, Hessel EM, Coffman RL (2007) Therapeutic targeting of innate immunity with Toll-like receptor agonists and antagonists. Nat Med 13:552–559.

Karikó K, Ni H, Capodici J, Lamphier M, Weissman D (2004) mRNA is an endogenous ligand for Toll-like receptor 3. J Biol Chem 279:12542–12550.

Khorooshi R, Owens T (2010) Injury-induced type I IFN signaling regulates inflammatory responses in the central nervous system. J Immunol 185:1258–1264.

Kigerl KA, Gensel JC, Ankeny DP, Alexander JK, Donnelly DJ, Popovich PG (2009) Identification of two distinct macrophage subsets with divergent effects causing either neurotoxicity or regeneration in the injured mouse spinal cord. J Neurosci 29:13435–13444.

Kim JB, Sig Choi J, Yu YM, Nam K, Piao CS, Kim SW, Lee MH, Han PL, Park JS, Lee JK (2006) HMGB1, a novel cytokine-like mediator linking acute neuronal death and delayed neuroinflammation in the postischemic brain. J Neurosci 26:6413–6421.

Lee MH, Wang T, Jang MH, Steiner J, Haughey N, Ming GL, Song H, Nath A, Venkatesan A (2011) Rescue of adult hippocampal neurogenesis in a mouse model of HIV neurologic disease. Neurobiol Dis 41:678–687.

Loiarro M, Sette C, Gallo G, Ciacci A, Fantò N, Mastroianni D, Carminati P, Ruggiero V (2005) Peptide-mediated interference of TIR domain dimerization in MyD88 inhibits interleukin-1-dependent activation of NF-κB. J Biol Chem 280:15809–15814.

Malmgaard L (2004) Induction and regulation of IFNs during viral infections. J Interferon Cytokine Res 24:439–454.

Miyanishi M, Tada K, Koike M, Uchiyama Y, Kitamura T, Nagata S (2007) Identification of Tim4 as a phosphatidylserine receptor. Nature 450:435–439.

Napoli I, Neumann H (2009) Microglial clearance function in health and disease. Neuroscience 158:1030–1038.

Neumann H, Kotter MR, Franklin RJ (2009) Debris clearance by microglia: an essential link between degeneration and regeneration. Brain 132:288–295.

Noppert SJ, Fitzgerald KA, Hertzog PJ (2007) The role of type I interferons in TLR responses. Immunol Cell Biol 85:446–457.

Okamura Y, Watari M, Jerud ES, Young DW, Ishizaka ST, Rose J, Chow JC, Strauss JF 3rd (2001) The extra domain A of fibronectin activates Toll-like receptor 4. J Biol Chem 276:10229–10233.

O'Neill LA, Bowie AG (2007) The family of five: TIR-domain-containing adaptors in Toll-like receptor signalling. Nat Rev Immunol 7:353–364.

Pais TF, Figueiredo C, Peixoto R, Braz MH, Chatterjee S (2008) Necrotic neurons enhance microglial neurotoxicity through induction of glutaminase by a MyD88-dependent pathway. J Neuroinflammation 5:43.

Pålsson-McDermott EM, O'Neill LA (2007) Building an immune system from nine domains. Biochem Soc Trans 35:1437–1444.

Park JS, Svetkauskaite D, He Q, Kim JY, Strassheim D, Ishizaka A, Abraham E (2004) Involvement of Toll-like receptors 2 and 4 in cellular activation by high mobility group box 1 protein. J Biol Chem 279:7370–7377.

Perry AK, Chen G, Zheng D, Tang H, Cheng G (2005) The host type I interferon response to viral and bacterial infections. Cell Res 15:407–422.

Pittock SJ, Lucchinetti CF (2007) The pathology of MS: new insights and potential clinical applications. Neurologist 13:45–56.

Ransohoff RM, Perry VH (2009) Microglial physiology: unique stimuli, specialized responses. Annu Rev Immunol 27:119–145.

Reed-Geaghan EG, Savage JC, Hise AG, Landreth GE (2009) CD14 and Toll-like receptors 2 and 4 are required for fibrillar Aβ-stimulated microglial activation. J Neurosci 29:11982–11992.

Rotshenker S, Reichert F, Gitik M, Haklai R, Elad-Sfadia G, Kloog Y (2008) Galectin-3/MAC-2, Ras and PI3K activate complement receptor-3 and scavenger receptor-AI/II mediated myelin phagocytosis in microglia. Glia 56:1607–1613.

Stevens B, Allen NJ, Vazquez LE, Howell GR, Christopherson KS, Nouri N, Micheva KD, Mehalow AK, Huberman AD, Stafford B, Sher A, Litke AM, Lambris JD, Smith SJ, John SW, Barres BA (2007) The classical complement cascade mediates CNS synapse elimination. Cell 131:1164–1178.

Stewart CR, Stuart LM, Wilkinson K, van Gils JM, Deng J, Halle A, Rayner KJ, Boyer L, Zhong R, Frazier WA, Lacy-Hulbert A, El Khoury J, Golenbock DT, Moore KJ (2010) CD36 ligands promote sterile inflammation through assembly of a Toll-like receptor 4 and 6 heterodimer. Nat Immunol 11:155–161.

Takahashi K, Rochford CD, Neumann H (2005) Clearance of apoptotic neurons without inflammation by microglial triggering receptor expressed on myeloid cells-2. J Exp Med 201:647–657.

Takahashi K, Prinz M, Stagi M, Chechneva O, Neumann H (2007) TREM2-transduced myeloid precursors mediate nervous tissue debris clearance and facilitate recovery in an animal model of multiple sclerosis. PLoS Med 4:e124.

Tanaka T, Ueno M, Yamashita T (2009) Engulfment of axon debris by microglia requires p38 MAPK activity. J Biol Chem 284:21626–21636.

Taylor AM, Jeon NL (2010) Micro-scale and microfluidic devices for neurobiology. Curr Opin Neurobiol 20:640–647.

Taylor AM, Blurton-Jones M, Rhee SW, Cribbs DH, Cotman CW, Jeon NL (2005) A microfluidic culture platform for CNS axonal injury, regeneration and transport. Nat Methods 2:599–605.

Teige A, Teige I, Lavasani S, Bockermann R, Mondoc E, Holmdahl R, Issazadeh-Navikas S (2004) CD1-dependent regulation of chronic central nervous system inflammation in experimental autoimmune encephalomyelitis. J Immunol 172:186–194.

Toshchakov VU, Basu S, Fenton MJ, Vogel SN (2005) Differential involvement of BB loops of Toll-IL-1 resistance (TIR) domain-containing adapter proteins in TLR4- versus TLR2-mediated signal transduction. J Immunol 175:494–500.

Trapp BD, Peterson J, Ransohoff RM, Rudick R, Mörk S, Bö L (1998) Axonal transection in the lesions of multiple sclerosis. N Engl J Med 338:278–285.

Vallières N, Berard JL, David S, Lacroix S (2006) Systemic injections of lipopolysaccharide accelerates myelin phagocytosis during Wallerian degeneration in the injured mouse spinal cord. Glia 53:103–113.

Vargas ME, Barres BA (2007) Why is Wallerian degeneration in the CNS so slow? Annu Rev Neurosci 30:153–179.

Voll RE, Herrmann M, Roth EA, Stach C, Kalden JR, Girkontaite I (1997) Immunosuppressive effects of apoptotic cells. Nature 390:350–351.

Wang J, Ren L, Li L, Liu W, Zhou J, Yu W, Tong D, Chen S (2009) Microfluidics: a new cosset for neurobiology. Lab Chip 9:644–652.

Wang R, Yang B, Zhang D (2011) Activation of interferon signaling pathways in spinal cord astrocytes from an ALS mouse model. Glia 59:946–958.

Yamamoto M, Sato S, Hemmi H, Sanjo H, Uematsu S, Kaisho T, Hoshino K, Takeuchi O, Kobayashi M, Fujita T, Takeda K, Akira S (2002a) Essential role for TIRAP in activation of the signalling cascade shared by TLR2 and TLR4. Nature 420:324–329.

Yamamoto M, Sato S, Mori K, Hoshino K, Takeuchi O, Takeda K, Akira S (2002b) Cutting edge: a novel Toll/IL-1 receptor domain-containing adapter that preferentially activates the IFN-β promoter in the Toll-like receptor signaling. J Immunol 169:6668–6672.

Yamamoto M, Sato S, Hemmi H, Hoshino K, Kaisho T, Sanjo H, Takeuchi O, Sugiyama M, Okabe M, Takeda K, Akira S (2003) Role of adaptor TRIF in the MyD88-independent Toll-like receptor signaling pathway. Science 301:640–643.

Zhang J, Jones M, DeBoy CA, Reich DS, Farrell JA, Hoffman PN, Griffin JW, Sheikh KA, Miller MI, Mori S, Calabresi PA (2009) Diffusion tensor magnetic resonance imaging of Wallerian degeneration in rat spinal cord after dorsal root axotomy. J Neurosci 29:3160–3171.

Zhang X, Goncalves R, Mosser DM (2008) The isolation and characterization of murine macrophages. Curr Protoc Immunol Chapter 14:Unit 14.1.

Ziegenfuss JS, Biswas R, Avery MA, Hong K, Sheehan AE, Yeung YG, Stanley ER, Freeman MR (2008) Draper-dependent glial phagocytic activity is mediated by Src and Syk family kinase signalling. Nature 453:935–939.

Zuluaga S, Gutiérrez-Uzquiza A, Bragado P, Alvarez-Barrientos A, Benito M, Nebreda AR, Porras A (2007) p38alpha MAPK can positively or negatively regulate Rac-1 activity depending on the presence of serum. FEBS Lett 581:3819–3825.